The Study of Aerodynamics and Productivity of the Savonius Rotor with Supplementary Blades

Mohanad Al-Ghriybah*, Ismail I. Hdaib*, Zakaria Al-Omari*‡, Yaseen Al-Husban*

*Department of Renewable Energy Engineering, Faculty of Engineering, Isra University, Amman-Jordan P.O.11622

(mohanad.alghriybah@iu.edu.jo, Ismail.hdaib@iu.edu.jo, zakaria.alomari@iu.edu.jo, Yaseen.alhusban@iu.edu.jo)

‡Zakaria Al-Omari; Isra University, P.O.11622 (Amman-Jordan), Tel: +90278 549 64 28, Fax: +9626 471 17 10, zakaria.alomari@iu.edu.jo

Received: 06.04.2022 Accepted:27.05.2022

Abstract- In this paper, the influence of the ends of the plates on the productivity of the Savonius wind turbine (SWT) with additional blades has been investigated numerically and experimentally. Initially, three-dimensional (3D) unsteady modeling is implemented for a turbine with and without endplates (EP), keeping the rotor dimensions fixed in both cases. Our simulation has been performed using the "k- Ɛ/realizable turbulence model" with the auxiliary of the "finite volume solver ANSYS Fluent 19.1". The coefficients of the torque and power "Cp and Ct" are estimated for any case depending on the tip speed ratio (TSR). The contours of velocity, stress, pressure, and disturbance strength are obtained and studded for the rotor with EP. Finally, a wind tunnel test is performed to prove the simulation results. The numerical results exposed that the highest value of Cp is 0.25 at TSR = 0.7 for the rotor with EP with an improvement of 26% over the same rotor without EP. Moreover, results proved that the maximum improvement in Cp for the rotor with EP was 38% at TSR = 0.4. However, the wind tunnel tests for the rotor with EP demonstrated the Cp max to be 0.226.

Keywords Savonius; inner blades; VAWT; endplates

1. Introduction

Over the past several decades, global warming has been rapidly worsening mainly due to the careless utilization of fossil fuels [1-7].

Sustainable energy sources have become a possible alternative to fossil fuels, which has increased the attention and demand for them around the world [8-16]. Recently, wind power considered as one of the most significant sources of clean and renewable energy [17, 18]. The available kinetic energy (KE) in the wind can be extracted using wind turbines (WTs) [19]. WTs are classified into two main categories, namely, horizontal-axis WTs and vertical-axis WTs (VAWTs).

VAWTs have several advantages over horizontal axis WTs. The main advantage is their comprehensive focus. Consequently, they can operate in any wind direction without requiring a yaw angle control system [20]. In addition, the gearbox and generator can be positioned at ground level to facilitate maintenance and reduce construction costs [21].

VAWTs are available in various types and sizes for several decades, as shown in "Figure 1", but they represent a small percentage of the world's operating WTs.

Fig. 1. Vertical axis WTs [17]

The Savonius wind turbine (SWTs), also called the "S-type rotor, was invented and patented by the Finnish engineer Sigurd Savonius". The turbine consists of two semi-cylindrical surfaces called blades, which are connected to a vertical shaft perpendicular to the wind direction.

The Savonius rotor (SR) has several positive qualities including the low cost of construction, simplicity of execution, the ability to operate in different directions of wind flow, low noise level, and most significantly a large starting aerodynamic momentum. But the SR has an important negative point - its low efficiency. Despite the fact that this

type of rotor has a large starting torque, during continuous operation, it can deliver a maximum power of no more than 5 kW.

A lot of research is currently underway to increase the efficiency of SRs including utilizing simulation programs and building mathematical models to study the aerodynamic properties of rotors; using hot air from natural heat sources or industrial residual heat to spin a turbine; using water energy instead of wind energy; In addition to a change in the design of the SWT.

SR with multi-stages has been tested by various researchers recently. It was observed that the multi-stage rotor could reduce the fluctuations in the generated moment without any loss in performance [22-24]. Other studies have focused on improving rotor performance by increasing the aspect ratio (AR). The AR is defined as the ratio between the diameter of the rotor and its height [25]. It was concluded that the high AR could increase the capacity of the rotor by reason of the reduction in the moment of inertia strength [26, 27]. On the other hand, innovations in blade profile optimization have been done in several studies. Elliptical profile was studied resulting in a higher coefficient of torque (Ct) and coefficient of power (Cp) compared to the traditional semi-circular rotor [28]. Authors of [29] examined a new design for the SR which is called the Bach rotor and found an improvement of 9% over the traditional rotor. [30] the Benesh-type rotor and found an enhancement of 15% compared to the traditional rotor.

Power augmentation techniques have been proposed in preceding studies such as deviant plates and windshields. Results showed an enhancement in terms of Cp and Ct; however, these techniques converted the rotor to be highly dependent on the wind direction [31, 32]. Additionally, several studies investigated the effect of blade quantity on the SWT productivity [33, 34]. They found that the addition of the blade on the traditional rotor reduces both Cp and Ct; this is due to the deflected air by the extra blades which will affect the performance of the following blade. Moreover, the influence of the overlap ratio on the aerodynamic capacity of the WT was investigated to obtain the optimal value of this ratio. Results showed that the optimal overlap ratio is in the range of $0 - 0.15$ [35]). The double blade rotor was had performed better than the traditional SR with a maximum improvement of 11.86% [36].

The influence of adding two inner blades (IB) to the traditional rotor at low rotational speed was executed by [37] using a two-dimensional (2D) simulation. They concluded that the IB was capable to catch the extra energy in the air which causes a rise in the rotor performance. Moreover, the influence of the supplemental blade's position on the performance of the SWT was studied by [38]. The researchers concluded that the best position is achieved when the tip of the IP is parallel to the rotor tip. The results observed for the SR by adding EP on the traditional and the helical rotors were adopted by various studies [39]. Utilizing EP, it was found that adding EP resulted in significant improvement of the Cp due to the reduction in the escaped air from the curved surface of the forward vane.

The main objective of our research is to examine the effect of using EP on the performance of SR with IB using 3D simulation (3DS) and experimental work, this modification can contribute to the enhance the performance of the rotor without increasing the cost of the rotor.

1.1. Objectives of the existing Study

The previous implementation requires a 3DS for the rotor with IBs in order to obtain more specifics about the flow structure around the rotor. With a goal of validation, the best-performed rotor proposed by a previous study [33] has been adopted. In the current study, EP has been adopted with the aim of increasing the Cp of the rotor. Initially, the unstable numerical simulations are executed with the influence of EPs using the "k- Ɛ/realizable turbulence model" with the help of "Ansys Fluent solver". Finally, the wind tunnel was rigorously tested to validate the simulation results

1.2. Geometry specifics

"Figure 2" illustrates the proposed configuration for the previous study [32] in a 2D view. A 3D configuration has been considered in the current study with and without EPs as shown in "Figure 3". The height of the rotor is adopted to be 600mm whereas the diameter and the thickness of EPs are adopted to be 0.4862m and 0.005m, respectively. The other dimensions are kept the same as the original configuration; the diameter of the major blade $= 0.188$m, the diameter of the IB$=$ 0144 m, the diameter of the shaft $=$ 0.03, and the IB angle $= 120^{o}$.

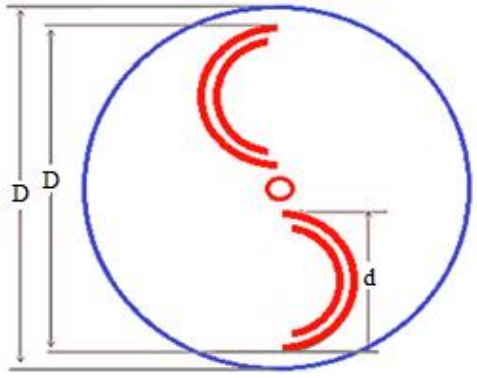

Fig. 2. Proposed rotor.

2. Mathematical Model

In the current study, CAD geometry is modeled using SOLIDWORKS software. The thickness of the blades is taken as 2 mm. The numerical domain is meshed using an unstructured grid. The main domain consisting of two sub-domains is divided using a sliding interface: a cylindrical sub-domain with rotational speed and a stationary cubic sub-domain. The diameter of the cylindrical sub-domain is taken as 0.5m and is placed at the center of the main domain. The dimensions of the domain are handled as "10D×10D×10D" where D is the rotor diameter. The domain is large in size in order to avoid the effect of wind tunnel blockage. The final adopted domain is shown in "Figure 4".

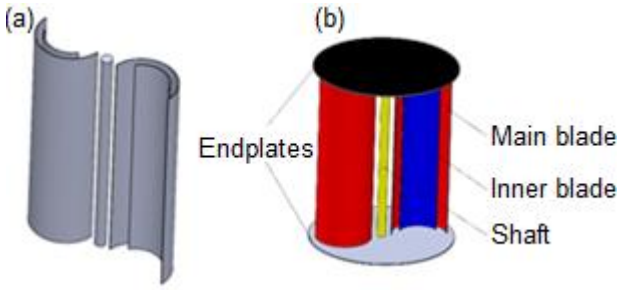

Fig. 3. (a) Rotor without EP; (b) Rotor with EP

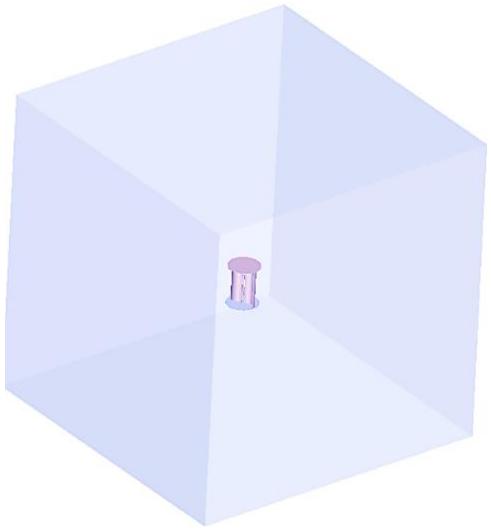

Fig. 4. Main numerical domain

For solving the flow with better accuracy at the boundaries of the blades, the inflation technique is used in order to provide layers with finer mesh on the edge of the blades. A total number of 25 layers are applied to the edges of the blades with a growth ratio rate of 1.2. The definitively adopted mesh for the cylindrical subdomain and the blades is shown in "Figure 5".

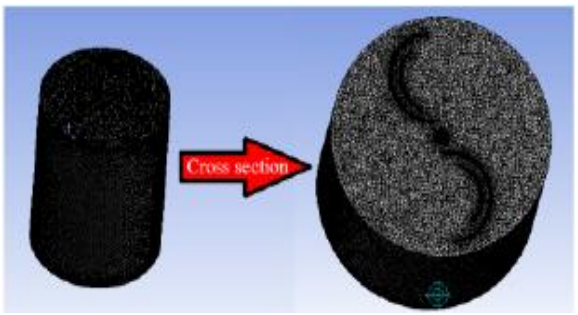

Fig. 5. Mesh for the cylindrical sub-domain and the blades

2.1. *Grid Autonomous Test*

A grid-autonomous test has been executed for the transient three-dimensional simulation. The test has been conducted by adopting three types of grids "coarse, medium, and fine". The different grid dimensions are shown in "Table 1".

Table 1. Cp for various types of the grid.

Grid type	Number of elements	Average Cp
Coarse	1,527,417	0.1145
Medium	3,383,145	0.1372
Fine	5,742,137	0.1387

It has been noticed that Cp for the medium and fine grid are roughly equal, so that, a medium grid with 3,383,145 elements is adopted for all the numerical simulations.

2.2. *Boundary Conditions*

The left side of the cubic main domain is set as an inlet "velocity inlet $= 9\mathrm{m/s}$" with a turbulent intensity of 5%. The opposite wall of the inlet is set as a pressure outlet. The other surfaces of the main domain are set to be stationary walls. A boundary condition with no gap applied to the surfaces of the blades. A sliding interface is set between the two sub-domains. The movement of the cylindrical domain is assigned with respect to the TSR by varying the values from 0.4 to 0.7.

2.3. *Turbulence Model and Solver Setup*

The turbulent flow around the SR is modeled by using the "k- Ɛ/realizable turbulence model". This model was utilized to predict the wall friction coefficient around the rotor with more accuracy [31]. The size of the time step for the simulations is determined based on five degrees of revolution/time step. The simulations are performed with 10 completed revolutions of the WT. The iterations per time step are set to be 20. With the aim of monitoring the convergence of the solution, the absolute criteria are utilized with a value of 10-5. The universal set of the fluent solver is set to be pressure-based. The semi-implicit method is used to create the coupling between pressure and velocity.

2.4. *Power and torque coefficients estimation*

The Cp of the SWR reflects the relation between the generated power by the WT and the total actual wind power and it can be expressed as follows:

$$Cp = \frac{P_{turbine}}{P_{available}} = \frac{P_{turbine}}{0.5\rho AV^3} \quad (1)$$

Ct for the simulation and the experiments can be expressed as follows:

$$Ct = \frac{T_{turbine}}{T_{available}} = \frac{T_{turbine}}{0.5\rho AV^2R} \quad (2)$$

where R is the radius of the rotor, V is the wind velocity, ρ is the density of air, and $\boldsymbol{A}$ represents the projected area of the rotor. The generated torque in the experiment work can be calculated as follows:

$$T_{turbine} = F \times r \quad (3)$$

Where F is the load on the pulley and r is the radius of the pulley. The relation between Ct and Cp can be expressed in terms of TSR as follows:

$$Cp = TSR \times Ct \tag{4}$$

3. Simulation results

Initially, a three-dimensional simulation is carried out for the proposed two-dimensional rotor [30]. The Cp values are estimated and plotted with respect to TSR. This step is also considered an important step in order to validate the 3DS with the published date. "Figure 6" shows the comparison between the 2D simulation and the 3DS for the same rotor. It can be observed from the figure that the 2D simulations share the same trend with a difference of less than 7%. The reliability and validity of the results of this study suggest that the results can be considered for further modeling processes.

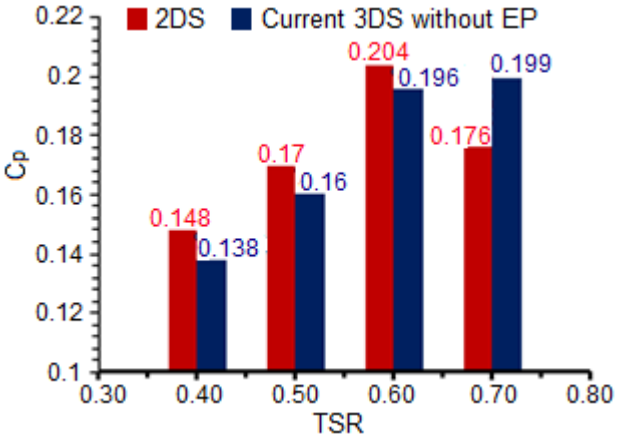

Fig. 6. Cp comparison between 2DS and 3DS

The results of the three-dimensional simulation for the rotor with EP are shown and compared in "Figure 7". It can be detected from the figure that the Cp of the turbine rotors enhances with the addition of EPs at all the considered values of TSR.

The peak value of Cp for the rotor with EPs is noticed to be 0.25 at TSR $= 0.7$, while at the same value of TSR, the peak value of Cp is found to be about 0.198 for the rotor without EP. This enhancement refers to the effect of EPs where those plates prevent the leakage of the air from the curved surface of the advancing blades (main and supplementary blades) to the outer flow maintaining the pressure difference between both blades at a suitable range. A maximum improvement with a percentage of 38% can be detected at 0.4 TSR for the turbine with EPs compared to the rotor without EPs whereas the overall percentage of improvement is about 25%. On the other hand, "Figure 8" shows a comparison in terms of Ct for both rotors with and without EPs. It can be observed from the figure that the spinning velocity of the blades decreases with the increase of the load and therefore, the value of Ct reduces together with the increase of TSR. Moreover, it can be noted that the Ct max is generated at the lowest considered value of TSR for the rotor with EPs.

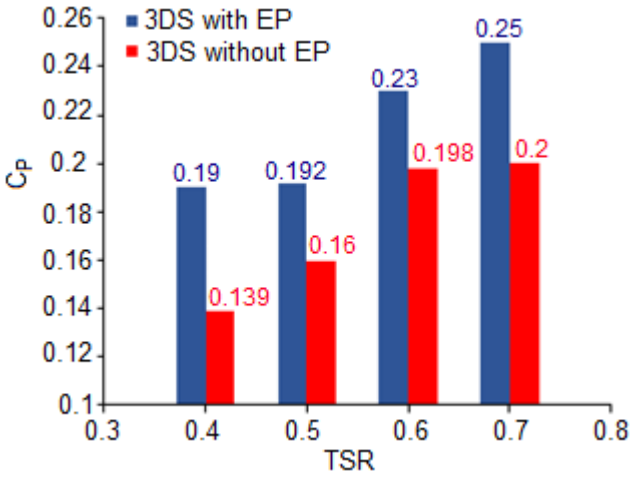

Fig. 7. Cp comparison for the rotor with and without EP

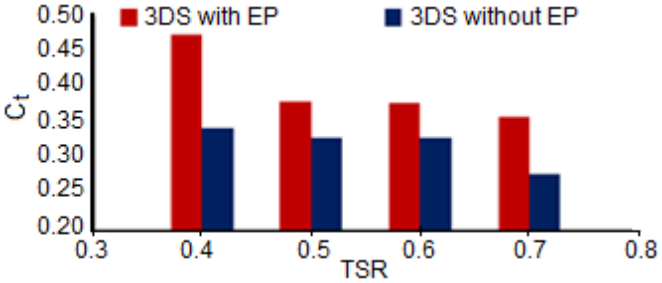

Fig. 8. Ct comparison for the rotor with and without EP

"Figure 9" illustrates the difference in pressure for the blades at TSR of 0.7 at several cross-sections to offer a further intelligible view regarding the distribution of the pressure where it can be seen that the curved surface of the forward blade has higher pressure on it and the cambered surface of the returning blade has lower pressure. This is because of the addition of EPs where the reflected air from the cambered surface of the forward blade is decreased which causes an increase in the upwind separation and so the air velocity behind the returning blade will be with higher values which are reduced the pressure behind the blade. Moreover, the symmetrical case can be observed at both lower and upper cross-sections where the pressure has similar values which shows that the top-EP and the bottom-EP have a similar influence on the rotor.

The distribution of the velocity around the turbine model in its 3D geometry is illustrated in "Figure 10". It can be observed from the distribution that the speed has higher values when moving from the shaft's center (center of rotation) to the direction of the outer surface of the blades. As the rotating speed of the turbine rises, the distribution of the speed nearby the turbine has a similar trend in magnitude, given that the blades are in a symmetrical condition. Regions with low speed reveal a region with high-pressure values. These regions appear with a blue color on the speed contours distribution. Moreover, it can be seen that the distribution of the velocity has the lowest value in the center of the EP and the highest value in the periphery of the EP.

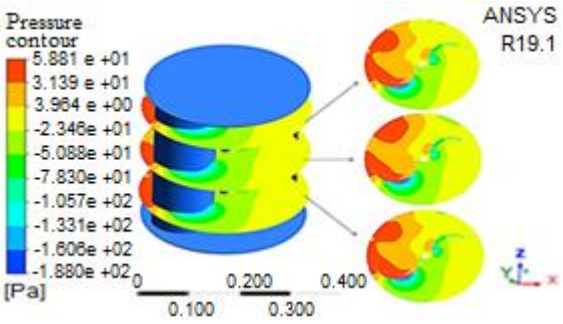

Fig. 9. Pressure contours at various cross-sections

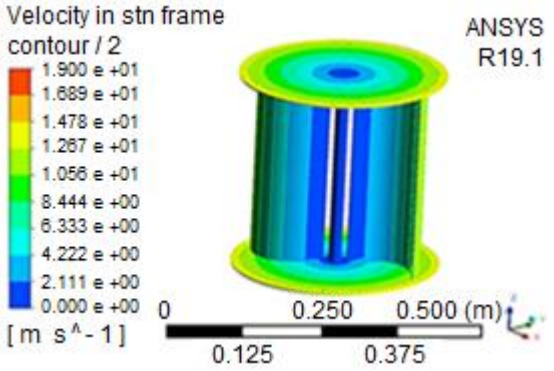

Fig. 10. Velocity contours at TSR = 0.7

Furthermore, wake effect and turbulence are highly 3D dependent. For that reason, "Figure 11" illustrates the turbulence KE for the proposed turbine at a TSR of 0.7. It can be noticed from the turbulence KE distribution that the turbulent KE has lower values at the inlet of the main domain, whereas, it has higher values on the turbine surface, particularly on the blade's edges.

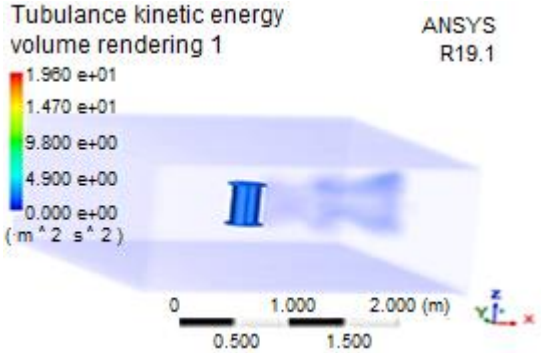

Fig. 11. Turbulence kinetic energy at TSR = 0.7

4. Empirical Investigation

The investigations are carried out for the SR with IB and EPs in an open-type test section wind tunnel at the aerodynamics laboratory to prove the simulated results.

4.1. Material and approaches

The wind tunnel test is performed for the fabricated rotor. The schematic diagram of the experimental arrangement and the actual design is shown in "Figure12". A centrifugal air fan which consists of 14 blades has been utilized. The turbine was positioned in front of the fan as an open circuit wind tunnel. The position of the WT was corrected so that any fluctuation of the flux stream may not affect the distributions of the speed and the stress in the direction of the rotation. Wind velocity is recorded utilizing an anemometer with ranges between 0.4 and 45 m/s with an accuracy of ±0.03. Wind speeds were diverse around 9 m/s to achieve a TSR value that ranges between 0.4 and 0.7 to study the efficiency of the rotor under, various values of TSR. Aiming to assess the rotor performance at different values of TSR, the output torque and output power have been measured and analyzed. The rotor rotational speed has been measured utilizing a "digital tachometer". Moreover, the generated torque by the turbine has been measured utilizing a mechanical system called "a rope brake dynamometer". A 1mm nylon string was affixed to a frictionless pulley on the main rotating shaft through which the cargo brake was affixed, and the other end of the nylon string was affixed to a mass-spring balance for measuring the spring readings and then calculating the mechanical torque.

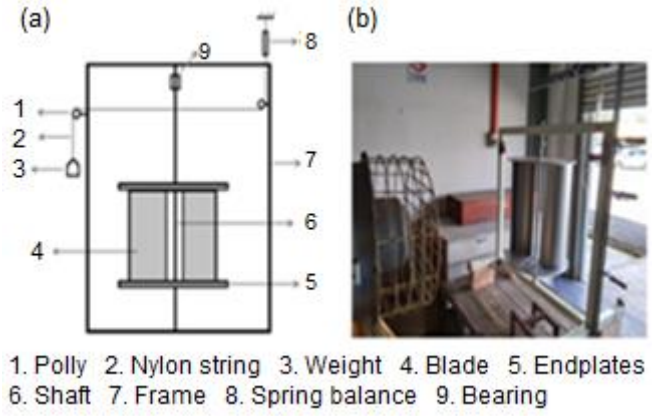

Fig. 12. (a) Schematic diagram of the experiment arrangement; (b) Actual arrangement

The galvanized iron was utilized in order to fabricate the turbine. The turbine dimensions are kept the same as the numerical model. A variac transformer is utilized in order to modify the voltage and therefore the exhaust fan speed.

A uniformity study for the air flux around the experimental model has been completed utilizing the fan anemometer. Various test points on the turbine model were adopted "First point P1; Second point P2 at the top of the rotor; Third point P3 at the center of the shaft; Fourth point P4; the Fifth point P5 at the bottom of the rotor" as illustrated in "Figure 13". A constant flux of air off a speed of 7 m/s. was applied to the model during the experiment.

Fig. 13. Uniformity wind test with five points

4.2. Experimental Results and Discussion

At the outset, the uniformity test results are illustrated in "Table 2". Results indicated that the air stream around the turbine was uniform flow where the maximum deviation was about 1.4% at the shaft's center.

Table 2. Results of wind speed using an anemometer.

Testing Point	Measured speed (m/s)	Deviation in wind speed
P1	7.2	0.0
P2	7.2	0.0
P3	6.9	0.15
P4	7.1	0.0
P5	7.1	0.0

Rotor speed in revolutions per minute (rpm) data is recorded for the tested turbine. The turbine is spinning freely without any load during the experiment. The rpm and wind velocity data are plotted and illustrated in "Figure 14". It can be seen from the plot that the self-starting characteristics of the turbine have been improved during the low speeds of wind. The turbine starts spinning at a wind speed of 2.8 m/s with a $rpm = 45$. In addition, "Figure 14" shows that the tested WT reaches a spinning velocity of 283 rpm when the wind velocity reaches 9 m/s.

From the wind test, the peak value of Cp the tested rotor is found to be 0.226 at TSR = 0.7 (Figure 15). Moreover, it is noticed in "Figure 16" that the torque values are reduced with the application of load. This is also can be noticed in the present CFD analysis.

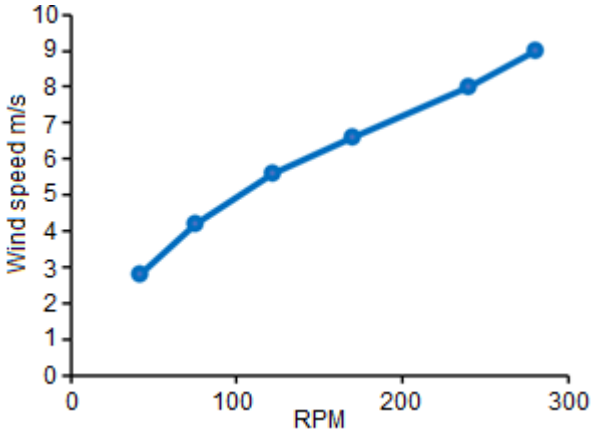

Fig. 14. RPM vs. wind velocity

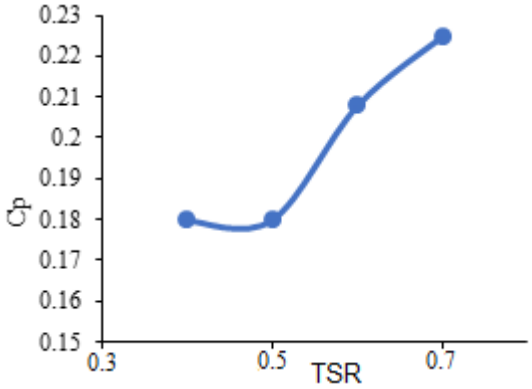

Fig. 15. Cp results from the wind tunnel test

The 3D unsteady results have been validated with the experimental results as shown in "Figure 16". The Cp values of the experiment are found to be very near to the Cp results from the 3D unsteady simulation. However, a deviation of 8% is found between the results. This is because of the losses involved in the wind tunnel test such as frictional losses between the shaft and the ball bearing, and measuring devices error such as "spring balance, tachometer, air velocity meter". Additionally, it can be noticed that the Cp curves from the two approaches (wind tunnel test and CFD simulation) are following the same trend "Figure 17".

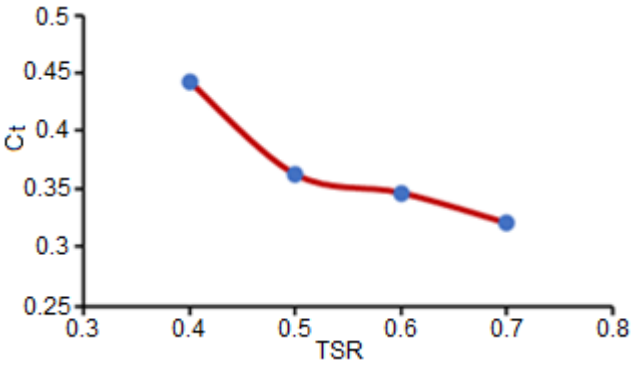

Fig. 16. Ct results from the wind tunnel test

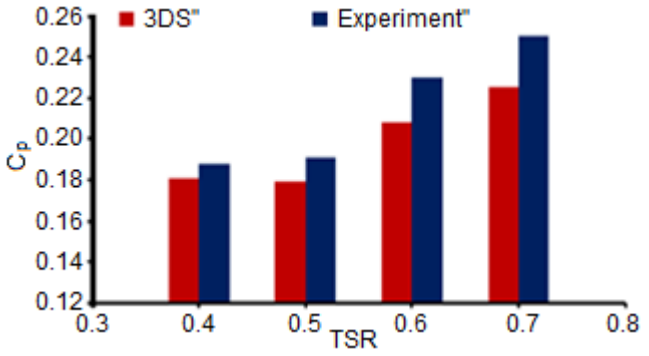

Fig. 17. Comparison of experimental and numerical results

5. Conclusion

In the current work, the influence of EP on the Productivity of the SWR with supplementary blades has been investigated using two approaches: empirical and numerical modeling. To begin with, 3D unsteady simulation is performed on the rotor with and without EP. Numerically, the rotor with EP shows a peak Cp of 0.25 at TSR = 0.7; while the rotor without EP shows a peak Cp of 0.198 at the same TSR.

The leakage of air from the concave side of the advancing air flux from IB is found to be less in the rotor with EP than in the same rotor without EP.

Thereafter, a wind tunnel test has been performed aiming to provide validation to the numerical results. The test shows that the highest Cp value is found to be 22.6%. Consequently, in the rotor with EP, there is an overall improvement of Cp by 25% over the same rotor without EP.

The effects of EPs with different types and scales on the SR with IB can be considered as future work.

References

[1] Frederica Perera, "Pollution from Fossil-Fuel Combustion is the Leading Environmental Threat to Global Pediatric Health and Equity: Solutions Exist," Int J Environ Res Public Health. Vol. 15, No 1, 2018 Jan; doi: 10.3390/ijerph15010016]

[2] Duli Chand Meena, Madhusudan Singh, Ashutosh K. Gir, "A Modified NLMS Control Algorithm for Coordinated Operation in Three-Phase Wind-Energy Conversion System," International Journal of Renewable Energy Research, vol. 11, no. 4, pp. 1621-1629, 2021.

[3] Mihir Mehta*‡, Dr. Bhinal Mehta, "Modified Rotor Flux Estimated Direct Torque Control for Double Fed Induction Generator," International Journal of Renewable Energy Research, vol. 12, no. 1, pp. 125-133, 2022.

[4] Julia Penfield, "Ultra Long-Term Wind Farm Generation Forecast by Combining Numerical Weather Prediction with Gated Recurrent Units," 9th International Conference on Smart Grid (icSmartGrid), IEEE, 2021.

[5] Yuto Iwasaki et al, "Basic study for the construction of a microgrid using small wind turbines as the main power source," 9th International Conference on Smart Grid (icSmartGrid), IEEE, 2021.

[6] Tufan Volkan Kucuk, Selim Oncu, "Wind Energy Conversion System with PDM Controlled Converter," 10th International Conference on Renewable Energy Research and Application (ICRERA), IEEE, 2021.

[7] Ryota Miyao et al, "A New Dynamic WPT Driven Capacitor Scooter System," 9th International Conference on Renewable Energy Research and Application (ICRERA), IEEE, 2020.

[8] M. Al-Ghriybah, F. Zulkafl, D. Hissein Didane, and S. A. Mohd, "wind energy assessment for the capital city of Jordan, Amman", Journal of Applied Engineering science, Vol. 17, No. 3, pp. 310–319, (2019).

[9] A. Hamzeh, S. Hamed, Z. Al-Omari, "First-Year Performance of a PV Plant in Jordan Compared to PV Plants in the Region," International Journal of Renewable Energy Research, vol. 5, no. 4, pp. 983-990, 2015.

[10] A. Hamzeh, Sadeq A. Hamed, Zakaria Al-Omari, "Wind Generation Impact on Symmetrical Fault Level at Grid Buses," International Journal of Electrical and Computer Engineering, vol. 8, no. 5, pp. 2682-2690, (2018).

[11] A. Hamzeh, Sadeq A. Hamed, Zakaria Al-Omari, "Design and Construction of a Small Stand-Alone Wind Turbine Using Scrap Materials," Renewable Energy and Sustainable Buildings, Ed. Ali Sayigh Springer International Publishing pp. 379-390, (2020).

[12] A Hamzeh, Z Alomari, "Grid Impacts of Full Interface Converter Wind Generation on Balanced Fault Response," GCREEDER, Amman-Jordan, September 10th– 12th, (2013).

[13] Tufan Volkan Kucuk, Selim Oncu, "Wind Energy Conversion System with PDM Controlled Converter," 10th International Conference on Renewable Energy Research and Application (ICRERA), IEEE, 2021.

[14] Faten AYADI, "Targets of Countries in Renewable Energy," 9th International Conference on Renewable Energy Research and Application (ICRERA), IEEE, 2020.

[15] G. Jackson, and D. Söffker, "State-of-the-art in wind turbine control: trends and challenges," Renewable and Sustainable Energy Reviews, vol. 60, pp. 377-393, 2016, doi: 10.1016/j.rser.2016.01.110

[16] Mohanad Al-Ghriybah, "Assessment of Wind Energy Potentiality at Ajloun, Jordan Using Weibull Distribution Function," Evergreen, vol. 9, no. 1, pp. 10–16, Mar. 2022.

[17] S. Sbramanian, C. Sankaralingam, R. M. Elavarasan, R. R. Vujayaraghavan, K. Raju, and L. Mihet-popa, "An evaluation on wind energy potential using multi-objective optimization based non-dominated sorting genetic

algorithm III," Sustainability, Vol. 13, No. 1, p. 410, 2021, doi: 10.3390/su13010410.

[18] M. M. A. Awan, M. Y. Javed, A. B. Asghar, K. Ejsmont, and Zia-ur-Rehman, "Economic Integration of Renewable and Conventional Power Sources—A Case Study," Energies, vol. 15, no. 6, p. 2141, Mar. 2022

[19] Mutharasan Anburaj, Chandrasekar Perumal, "Fatigue mitigation of wind turbine system using multiple point model predictive control," International Journal of Power Electronics and Drive Systems (IJPEDS), Vol. 12, No. 4, pp2261-2272, December 2021, DOI: 10.11591/ijped.

[20] M. Al-Ghriybah, M. Fadhli Zulkafli, D. Hissein Didane, and S. Mohd, "The effect of spacing between inner blades on the performance of the Savonius wind turbine," Sustain. Energy Technol. Assessments, vol. 43, p. 100988, Feb. 2021.

[21] M. Al-Ghriybah, M. F. Zulkafli, D. H. Didane, and S. Mohd, "The effect of inner blade position on the performance of the Savonius rotor," Sustain. Energy Technol. Assessments, vol. 36, p. 100534, Dec. 2019.

[22] H. Peimani, "Appropriate Technologies for Removing Barriers to the Expansion of Renewable Energy in Asia: Vertical Axis Wind Turbines". ADBI Working Paper 1250. Tokyo: Asian Development Bank Institute. 2021.

[23] U. K. Saha, S. Thotla, and D. Maity, "Optimum design configuration of Savonius rotor through wind tunnel experiments," J. Wind Eng. Ind. Aerodyn., vol. 96, no. 8–9, pp. 1359–1375, Aug. 2008.

[24] S. Frikha, Z. Driss, E. Ayadi, Z. Masmoudi, and M. S. Abid, "Numerical and experimental characterization of multi-stage Savonius rotors," Energy, vol. 114, pp. 382–404, Nov. 2016.

[25] M. Al-Ghriybah, M. F. Zulkafli, D. H. Didane, and S. Mohd, "Performance of the Savonius Wind Rotor with Two Inner Blades at Low Tip Speed Ratio," CFD Lett., vol. 12, no. 3, pp. 11–21, Mar. 2020.

[26] A. Kumar and R. P. Saini, "Numerical investigation and novel designing of multi-stage savonius rotor for harnessing hydropower," in 2015 Annual IEEE India Conference (INDICON), pp. 1–6, 2015.

[27] V. Patel, G. Bhat, T. I. Eldho, and S. V. Prabhu, "Influence of overlap ratio and aspect ratio on the performance of Savonius hydrokinetic turbine," Int. J. Energy Res., vol. 41, no. 6, pp. 829–844, May 2017.

[28] M. Zemamou, M. Aggour, and A. Toumi, "Review of savonius wind turbine design and performance," Energy Procedia, vol. 141, pp. 383–388, Dec. 2017.

[29] N. Alom and U. K. Saha, "Influence of blade profiles on Savonius rotor performance: Numerical simulation and experimental validation," Energy Convers. Manag., vol. 186, pp. 267–277, Apr. 2019.

[30] I. Ushiyama, H. Nagai, and J. Shinoda, "Experimentally Determining the Optimum Design Configuration for Savonius Rotors," Bull. JSME, vol. 29, no. 258, pp. 4130–4138, 1986.

[31] H. R. Rahai, "Development of optimum design configuration and performance for vertical axis wind turbine: feasibility analysis and final EISG report 2005.," USA, 2015.

[32] M. Al-Garibay, M. F. Zulkafli, D. H. Didane, and S. Mohd, "Review of the Recent Power Augmentation Techniques for the Savonius Wind Turbines," J. Adv. Res. Fluid Mech. Therm. Sci., vol. 60, no. 1, pp. 71–84, 2019.

[33] S. P. Venkatesan, S. Venkatesh, M. Sunil Kumar, S. Senthamizh Selvan, and Y. Sai, "Analysis of the blade profile of the Savonius wind turbine using computational fluid dynamics," Int. J. Ambient Energy, pp. 1–7, Jun. 2019.

[34] F. Wenehenubun, A. Saputra, and H. Sutanto, "An Experimental Study on the Performance of Savonius Wind Turbines Related with The Number of Blades," Energy Procedia, vol. 68, pp. 297–304, Apr. 2015.

[35] W. A. El-Askary, M. H. Nasef, A. A. Abdel-Hamid, and H. E. Gad, "Harvesting wind energy for improving the performance of Savonius rotor," J. Wind Eng. Ind. Aerodyn., vol. 139, pp. 8–15, Apr. 2015.

[36] M. Al-Garibay, M. F. Zulkafli, D. H. Didane, and S. Mohd, "Performance of Double Blade Savonius Rotor at Low Rotational Speed," J. Comput. Theor. Nanosci., vol. 17, no. 2, pp. 729–735, 2020.

[37] K. S. Jeon, J. I. Jeong, J.-K. Pan, and K.-W. Ryu, "Effects of end plates with various shapes and sizes on helical Savonius wind turbines," Renew. Energy, vol. 79, pp. 167–176, Jul. 2015.

[38] M. Al-Ghriybah, M. F. Zulkafli, and D. H. Didane, "Numerical Investigation of Inner Blade Effects on the Conventional Savonius Rotor with External Overlap," J. Sustain. Dev. Energy, Water Environ. Syst., vol. 9, no. 2, 2022.

[39] S. A. Farshad and M. Sheikholeslami, "Simulation of exergy loss of nanomaterial through a solar heat exchanger with insertion of multi-channel twisted tape," Journal of Thermal Analysis and Calorimetry volume., vol. 138, no. 1, pp. 795–804, Oct. 2019.